Cross-beta Order and Diversity in Nanocrystals of an Amyloid-forming Peptide

Ruben Diaz-Avalos[1]*, Chris Long[1], Eric Fontano[1], Melinda Balbirnie[2] Robert Grothe[2], David Eisenberg[2] and Donald L. D. Caspar[1]

[1]*Institute of Molecular Biophysics, Florida State University, Tallahassee, FL 32306, USA*

[2]*HHMI and Molecular Biology Institute, UCLA, Los Angeles CA 90095-1570, USA*

The seven-residue peptide GNNQQNY from the N-terminal region of the yeast prion protein Sup35, which forms amyloid fibers, colloidal aggregates and highly ordered nanocrystals, provides a model system for characterizing the elusively protean cross-beta conformation. Depending on preparative conditions, orthorhombic and monoclinic crystals with similar lath-shaped morphology have been obtained. Ultra high-resolution (<0.5 Å spacing) electron diffraction patterns from single nanocrystals show that the peptide chains pack in parallel cross-beta columns with ~ 4.86 Å axial spacing. Mosaic striations 20–50 nm wide observed by electron microscopy indicate lateral size-limiting crystal growth related to amyloid fiber formation. Frequently obtained orthorhombic forms, with apparent space group symmetry $P2_12_12_1$, have cell dimensions ranging from $|a| = 22.7-21.2$ Å, $|b| = 39.9-39.3$ Å, $|c| = 4.89-4.86$ Å for wet to dried states. Electron diffraction data from single nanocrystals, recorded in tilt series of still frames, have been mapped in reciprocal space. However, reliable integrated intensities cannot be obtained from these series, and dynamical electron diffraction effects present problems in data analysis. The diversity of ordered structures formed under similar conditions has made it difficult to obtain reproducible X-ray diffraction data from powder specimens; and overlapping Bragg reflections in the powder patterns preclude separated structure factor measurements for these data. Model protofilaments, consisting of tightly paired, half-staggered beta strands related by a screw axis, can be fit in the crystal lattices, but model refinement will require accurate structure factor measurements. Nearly anhydrous packing of this hydrophilic peptide can account for the insolubility of the crystals, since the activation energy for rehydration may be extremely high. Water-excluding packing of paired cross-beta peptide segments in thin protofilaments may be characteristic of the wide variety of anomalously stable amyloid aggregates.

© 2003 Elsevier Ltd. All rights reserved

Keywords: amyloids; cross-beta; powder diffraction; electron diffraction; prions

*Corresponding author

Introduction

The cross-beta polypeptide conformation is characteristic of the pathological amyloid fiber aggregates associated with various neurodegenerative diseases, including Alzheimer's, Huntington's, Parkinson's, and systemic amyloidoses. This fibrous protein folding, in which the beta strands are directed across the fiber axis, was first identi-

fied in X-ray diffraction patterns from oriented specimens of denatured globular[1] and fibrous[2] proteins. In contrast to the familiar fibrous proteins consisting of extended α-helices (e.g. keratin, myosin and fibrin), collagen triple helices or β-strands (e.g. silks), the cross-beta conformation is rare among naturally occurring biological fibers.[3] Cross-beta appears to be a dead-end for protein folding. These protease-resistant fibrous aggregates can be formed by proteins and peptides with uncorrelated amino acid composition and sequence by self-nucleated self-assembly. However, beyond the evident similarities observed in

E-mail address of the corresponding author: diaz@sb.fsu.edu

the diffraction patterns from cross-beta fibrils formed by a wide variety of proteins and peptides, little is known about the atomic structure of amyloid aggregates that can account for their pathological stability and self-propagating properties.

The characteristic signature of the cross-beta fiber diffraction pattern is a sharp 4.7–4.9 Å meridional maximum, usually accompanied by a ~10 Å equatorial reflection, strongly suggestive of a β-sheet structure oriented with the polypeptide chains perpendicular to the fiber axis. The absence of a ~9.6 Å layer-line spacing in the diffraction patterns of most amyloids indicates a tendency to a parallel β-sheet structure; however, due to the disorder in these specimens, the antiparallel structure cannot be excluded. Synthetic peptides corresponding to some portions of amyloidogenic proteins assemble into fibers with all the amyloid characteristics.[4] In particular, peptides from the Alzheimer's amyloid Aβ-protein form cross-beta fibrils, but different fragments have shown both parallel[5] and antiparallel β-sheet structure.[6,7] The presumption is then that the Aβ amyloid fibrils may contain both parallel and antiparallel β-sheets.

The best characterized cross-beta structure is the egg-stalk of the green lace-wing fly, *Chrysopa flava*. The X-ray fiber pattern[8] clearly shows the 9.48 Å spacing diagnostic of the antiparallel β-sheet, but diffraction on this layer-line is weak compared to the 4.74 Å layer-line marking the hydrogen-bonded chain separation. An atomic model for the peptide backbone was constructed, but the Chrysopa silk pattern does not provide sufficient information to define the atomic structure. It is evident that even with simple amyloid-forming peptides, using a variety of biophysical tools, it is proving difficult to obtain detailed information about the cross-beta atomic structure that can be related to biologically critical properties of amyloid.

The synthetic heptapeptide GNNQQNY from the prion determinant sequence of the yeast Sup35 protein forms a gel that shows all the characteristics of amyloid aggregates, and crystallizes spontaneously in aqueous solutions.[9] Addition of water produces two different crystal forms, depending on the previous history of the peptide. This peptide provides a model system to study the interactions that characterize the cross-beta structure at atomic resolution.

Results

Crystallinity, polymorphism and solubility of peptide aggregates

X-ray powder patterns of the anhydrous peptide dried from the ether precipitate following synthesis or from the column eluate in ~19% (v/v) acetonitrile showed an amorphous structure. Mixed with water at a concentration <5 mg/ml,

the peptide dissolved to form a stable solution with no observable aggregation after more than a year. At a concentration of 10 mg/ml, the initially clear peptide solution formed clumps after about a week, which yielded crystalline X-ray powder patterns with a very strong ~4.8 Å ring. Seeding with previously formed crystalline clumps shortened the time for visible precipitation to a few hours. At concentrations greater than ~20 mg/ml the peptide formed a viscous gel within ~30 minutes, which showed the characteristic green birefringence of amyloid when stained with Congo red. X-ray patterns collected from these gels showed the ~4.8 Å reflection expected from amyloid, with no sharp crystalline reflections. Once the aggregates have formed, whether crystalline or amyloid-like, they are stable to dilution with water, but can be dissolved in 5 M guanidinium hydrochloride or alkaline solution at pH 10.

Electron microscopy and diffraction display the diversity of structures among the peptide aggregates. Fibers, sheets, and elongated crystallites (nanocrystals) (Figure 1A–C) have been observed together in some specimens, although the crystallites predominated in specimens prepared at 10 mg/ml and were absent from fibrous gels at 20–50 mg/ml. The width and thickness of the nanocrystals range from ~20 nm to ~1 μm and the lengths are generally at least an order of magnitude greater than the width. The crystallinity of these elongated particles is vividly evident from their electron diffraction patterns, which can be recorded from specimens of width <200 nm. Many specimens show what appear to be single-crystal diffraction patterns, and when recorded
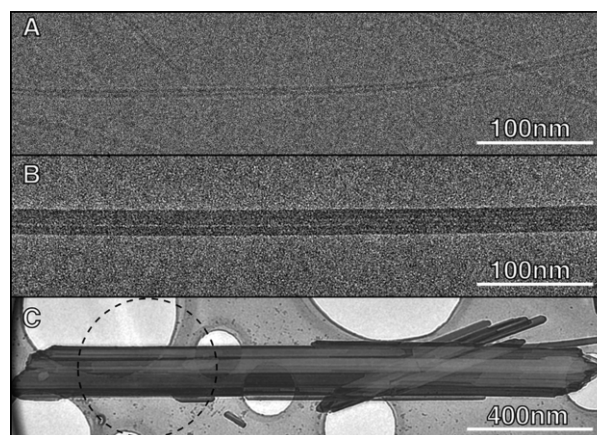

Figure 1. Aggregates formed after polymerization of GNNQQNY with water. A, Ice-embedded fibers formed at peptide concentrations greater than ~20 mg/ml. The diameter of the fibers is ~80 Å. B, Sheets co-existing with the crystals in suspensions formed at about 10 mg/ml. The sheets seem to consist of ~five protofilaments, each about 44 Å wide. C, Crystal showing striations along the large crystal dimension. The periodicity of the crystal along its long axis is 4.86 Å. The circled region was used to collect the diffraction pattern shown in Figure 2D.

with a suitably short camera length, discrete Bragg reflections extending beyond 0.5 Å spacing have been observed (Figure 2A and B). The layer-line spacing in all the diffraction patterns (Figure 2A–F) is ~4.85 Å, indicating that the heptapeptide molecules are all arranged in parallel β-sheets, with their hydrogen bonds directed along the long axis of the specimens, which corresponds to the fiber axis of the amyloid cross-beta structure.

Strong low-resolution inelastic scattering, as evident in Figure 2A, is characteristic of all the electron diffraction patterns. Because the Bragg reflections are sharp features, the inelastic scattering can be systematically removed either by measurements between the layer-lines (Figure 2C), or by high-pass filtering (Figure 2B and D–F). The Laue zones, clearly evident in Figure 2A and B, are nearly straight lines because the sphere of reflection for the 0.01644 Å wavelength electrons is nearly flat to atomic resolution. Indexing the spots along the slightly curved Laue zones defines the crystal orientation relative to the electron beam. For the nanocrystalline specimen that produced the pattern in Figure 2A and B, its b and c axes were tilted relative to the sphere of reflection, respectively, by ~8° in the horizontal direction and ~2° in the vertical direction. The width of the Laue zones depends sensitively on the profile of the Bragg reflections normal to the surface of the sphere of reflection. In Figure 2A and B, the reflections extend by about a third of the a^* reciprocal lattice spacing.

Accurate measurement of the reciprocal lattice spacings were made, as illustrated in Figure 2C, by recording the electron diffraction pattern from selected nanocrystals on a grid coated with ultra-fine evaporated gold particles to provide an internal spacing standard. A long camera length was used to enhance the order-to-order resolution. The pattern in Figure 2C shows that this specimen was oriented with both it's a and c axes very nearly perpendicular to the beam. The absence of odd-order reflections along these axes indicates the presence of 2-fold screw symmetry.

The diffraction pattern in Figure 2D, which was recorded from the circled portion of the specimen in Figure 1C, shows all the characteristics of a highly ordered single crystal. However, the striations evident in the electron micrograph of this specimen indicate that it consists of aligned long, thin crystallite domains, whose diameter may be comparable to the 20–30 nm wide crystals associated with this 180 nm wide specimen. Narrow fibrous crystalline domains with some

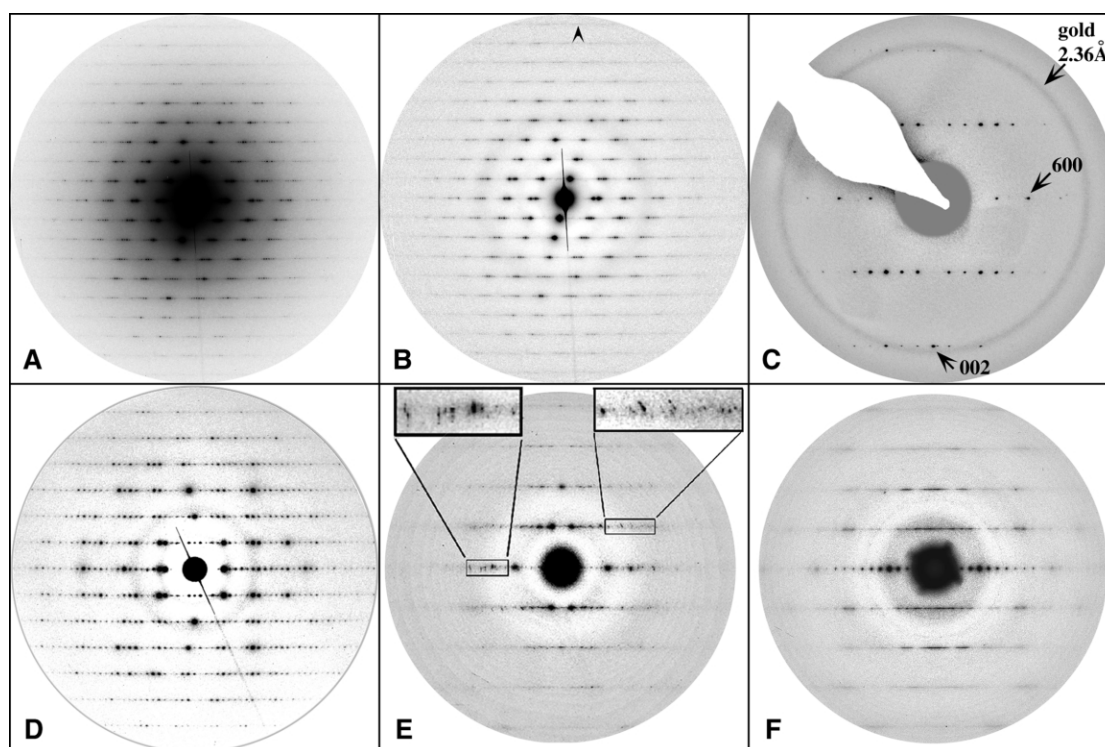**Figure 2**. Gallery of electron diffraction patterns. The spacing between horizontal planes is 1/4.86 Å in all cases. A, High-resolution pattern of a crystal before background subtraction. B, Pattern shown in A after background subtraction. The arrowhead near the top of the pattern indicates a reflection corresponding to ~0.53 Å. C, Pattern showing the systematic absence of reflections along the a^* and c^* axes. The ring of intensity near the edge of the pattern is due to evaporated gold used as calibration standard. D, Pattern from the crystal shown in Figure 1D. The Bragg reflections appear to arise from a single crystal, and extend to relatively high resolution (~0.7 Å). E, Diffraction pattern showing the presence of multiple mosaic domains with nearly the same orientation. F, Diffraction pattern showing colloidal crystalline order. There is strong sampling in the equator, indicative of a regular arrangement of protofibrils in the plane perpendicular to the long axis of the crystal, but with random azimuthal orientations.

mosaic spread can account for the width of the Laue zones seen in Figure 2A, B and D.

Nanocrystalline specimens, whose shapes were not as uniform as that in Figure 1C, gave diffraction patterns such as that in Figure 2E. This pattern shows obvious polycrystalline character, with the mean orientation of the c axis of the crystallite domains very near perpendicular to the beam. Absence of diffracted intensity on the meridian of the first layer-line again indicates 2-fold screw axis along c.

Specimens that have less sharply defined edges than the evident lath-shaped crystals yielded diffraction patterns such as that in Figure 2F. The sharp equatorial Bragg reflections with a 21.2 Å periodicity, together with a continuous intensity distribution on the off-equatorial layer-lines, indicate a columnar crystalline colloidal structure. If the equatorial reflections correspond to the (1,1) direction of a two-dimensional hexagonal lattice, the specimen would consist of hexagonally packed protofilaments of 42.4 Å diameter. This dimension is similar to the width of the protofilaments of the two-stranded fiber and five-stranded sheet in Figure 1A and B, respectively. If the equatorial reflections correspond to a (1,0) hexagonal lattice direction, the protofilaments would have a diameter of 24.5 Å. Whatever the diameter of the protofilaments in these colloidal crystalline specimens, the ~4.9 Å layer-line spacing (Figure 2F) shows that the heptapeptides are connected in a cross-beta structure very similar to that of the crystalline specimens, but without long-range axial alignment of the strands.

Cell dimensions and symmetry of orthorhombic specimens

Absence of odd-order reflections along the principal lattice axes of the orthorhombic unit cell, as generally observed in electron diffraction patterns of appropriately aligned nanocrystals (e.g. Figure 2C), indicates that the space group is $P2_12_12_1$. However, weak odd-order $h00$, $0k0$ and $00l$ reflections are sometimes observed in strong exposures, which may be due to secondary electron scattering effects or non-integral repeats within the nanocrystalline domains.[10] Furthermore, some patterns recorded with high order-to-order resolution, show the presence of weak satellites associated with the Bragg reflections in the ~4.9 Å spacing layer planes, which may be due to perturbations in the lateral packing of the cross-beta columns with periodicities incommensurate with the a and b cell dimensions. Whatever the source of the "forbidden" reflections, it is evident from the strong diffracted intensities that the density distribution of the four molecules in the orthorhombic unit cell appears half-staggered when projected along the principal axes, which can be accounted for by the orthogonal screw axes of the $P2_12_12_1$ space group.

Previous measurements by X-ray powder diffraction of an orthorhombic crystalline specimen[9] gave cell dimensions of $a = 22.63$ Å, $b = 39.44$ Å and $c = 4.86$ Å (after re-indexing the strong 4.72 Å spacing reflection as the 021, as established from our single-crystal electron diffraction data). Density measurements on this specimen confirmed that the four heptapeptide molecules in the unit cell are tightly packed, constituting more than 90% of the cell mass. It was therefore surprising to observe by electron diffraction that the a axis of different highly ordered crystals varied from 22.7 Å to 21.2 Å, depending on whether the specimen had been initially fast frozen or exposed to the electron microscope vacuum prior to cooling. Within the calibration uncertainty of the electron diffraction data from the gold standard, the c axis appeared constant at $4.87(\pm 0.02)$ Å. From the limited electron diffraction measurements of the b axis spacing (due to infrequent orientation of crystals with their b axis nearly perpendicular to the beam), this ~39.4 Å spacing did not appear to vary by more than ~1%. Thus, the 1.5 Å shrinkage of the a axis under extreme dehydrating conditions corresponds to a volume decrease per peptide molecule of 70 Å^3, which is comparable to the 60 Å^3 occupied by two liquid water molecules.

X-ray powder patterns (e.g. Figure 3) recorded from polycrystalline specimens of the heptapeptide, prepared under a variety of conditions, provided accurate lattice constant measurements, averaged over the agglomerations for comparison with the electron diffraction data from single nanocrystals. The X-ray data for the orthorhombic crystal form, summarized in Table 1, show dehydration-dependent shrinkages of the a axis by ~4% at 100 K and up to ~6% at room temperature, together with variations of ~1% or less in the b and c axes, which were not systematically correlated with drying. These changes are similar to those observed by electron diffraction, although the ~7% shrinkage of the a axis from the cryocooled nanocrystals in the ultra-high vacuum of the electron microscope was greater than that measured for the bulk specimens at 100 K and atmospheric pressure. Replacing water with ethanol or acetone in specimen A (Table 1) had little effect on the cell dimensions, but cooling this specimen in ethanol produced a 4% shrinkage of the a axis, which is similar to that of drying, while cooling of this specimen when wet decreased a by only 1%. Remarkably, specimen B (Figure 3, Table 1), which was prepared by the same protocol as specimen A, has significantly different lattice constants compared to A, both wet and dry, corresponding to volume decreases per peptide molecule on dehydration of ~28 Å^3 for B and ~72 Å^3 for A. These volume changes for each specimen were measured to be reversible, since adding water to the dried specimens returned the lattice constants to those of their wet state. Although there are significant polymorphic differences among similarly prepared specimens, the
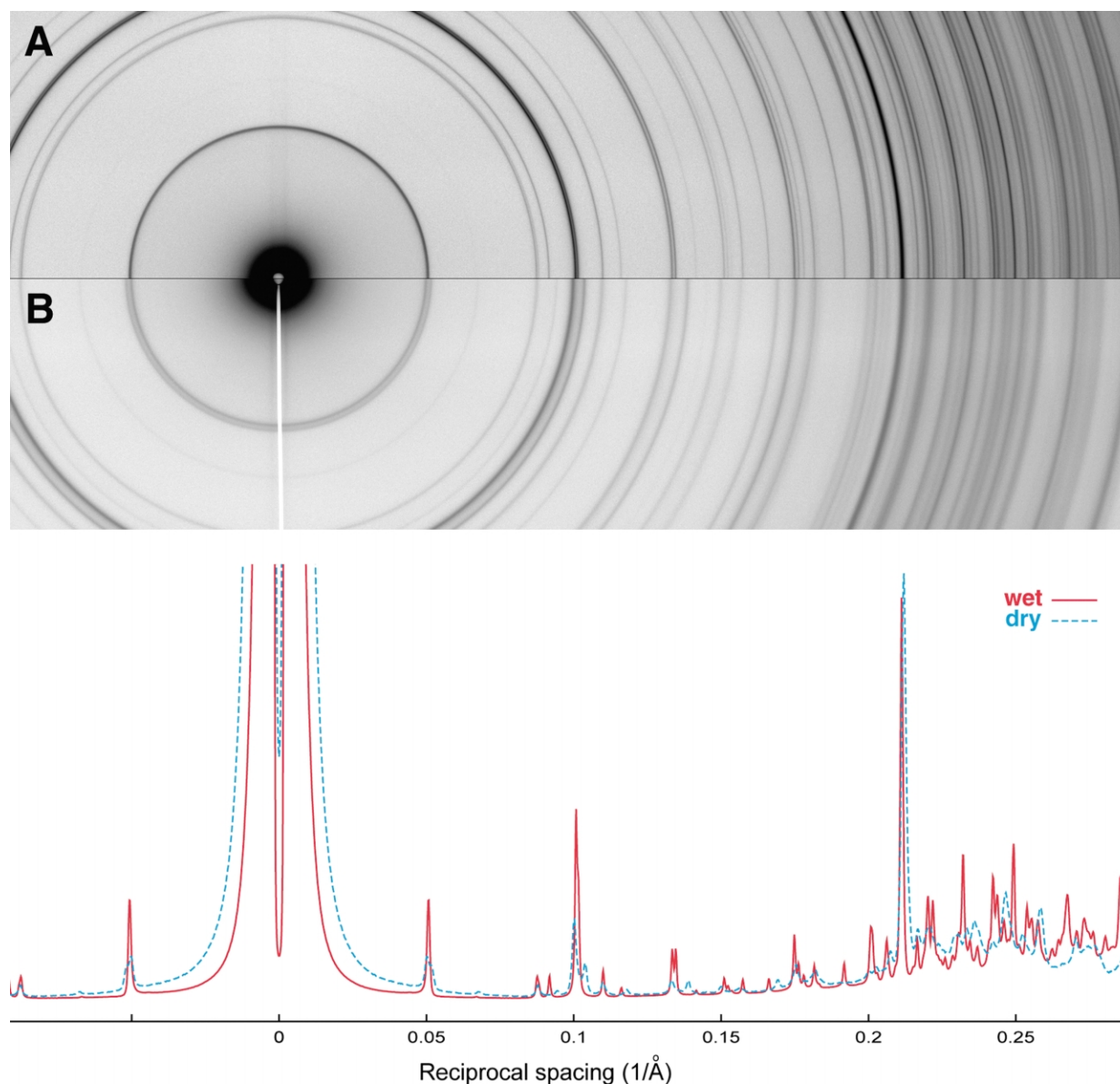
Figure 3. X-ray powder patterns of wet and dry specimens collected at the Spring8 synchrotron, using a camera with a cylindrical geometry in which the sample lies at the axis of the cylinder. The camera length was 1000 mm. The top half of the diffraction pattern (A) corresponds to the wet state, while the bottom half is from the dried specimen. B, Line traces of the two patterns. The strongest peak (at 0.2057 Å^{-1}) is due to the 021 reflection. The dried specimen shows more scattering at small angles than the wet, indicating a decrease in the coherence length of the crystals upon dehydration.

population in individual specimens appears quite homogeneous: analysis of the shapes of the Bragg reflections from powder patterns collected using a synchrotron source with high order-to-order resolution shows that the width of the reflections increases only marginally with resolution, contrary to the substantial broadening or splitting that would be observed with a heterogeneous sample.

Specimens crystallized from the amorphous ether precipitate of the heptapeptide, prior to the reverse phase chromatography usually employed for purification, gave X-ray powder patterns that show the formation of a crystal structure whose structure in both wet and dry state is distinctly different from that of the orthorhombic crystals (data not shown). The volume of this cell is similar to that of the orthorhombic form and presumably consists of an alternate packing of the four hepta-peptides with two non-equivalently related molecules in the crystallographic asymmetric unit. Electron diffraction patterns from single nano-crystal specimens of this polymorph demonstrate that the parallel cross-beta sheet packing with ~4.9 Å period *c* axis is very similar to that in the orthorhombic crystals. No three-dimensional electron diffraction data have been collected from this crystal form.

Table 1. Unit cell values under different environmental conditions

Temperature (K)		Solvent	a (Å)	b (Å)	c (Å)	V (Å³)
300 (X-rays)	A	Acetone	23.06	39.94	4.87	4490
		Ethanol	22.98	39.88	4.89	4479
		Water	22.93	39.95	4.89	4480
		Dried	21.65	39.84	4.86	4192
	B	Water	22.78	39.84	4.88	4429
		Dried	22.03	40.16	4.87	4309
100 (X-rays)		Water[a]	22.6	39.4	4.88[a]	4345
		Ethanol	21.97	39.95	4.8	4283
		Water	22.69	39.68	4.87	4384
		Dried	21.78	39.29	4.86	4159
100 (electrons)		Glucose (slow frozen)	21.2 ± 0.2	39.4 ± 0.24	4.87 ± 0.02	4068 ± 78
		Glucose	21.8 ± 0.3	39.4 ± 0.3	4.87	4189
		Glucose (fast frozen)	22.7 ± 0.2	39.4 ± 0.3	4.88 ± 0.02	4353

[a] Indexing the strongest reflection as 021.

Shape of reflections in reciprocal space

We attempted to process the electron diffraction data using software available for X-ray crystallography, i.e. Denzo[11] and MOSFLM.[12] However, these programs make the assumption that the Bragg reflections are point-like, producing unreliable results in our case. We attempted to map the data to reciprocal space assuming an oblate spheroidal shape for the Bragg reflections,[13] but these simulations proved unsatisfactory, due to the fact that the reflections have an unpredictable shape due to the mosaic crystal structure. Since the electron diffraction data consist of still images, each pattern represents a thin spherical shell of reciprocal space. In order to find the best rotation matrix, it was necessary to refine parameters including the camera length (magnification), the location of the crystal axes relative to the rotation axis of the sample stage of the microscope, and the center of each diffraction pattern. Although the variation in these parameters was relatively small (less than 1%), it was important to take these variations into account in order to have self-consistent data. Considering that the hydrogen bonding of the beta sheets in the crystals occurs along the c-axis, the side-chains of the seven amino acid residues should lie close to the $a-b$ plane of the crystal, and therefore, the most useful structural information is in the $hk0$ plane. Once the rotation matrices were calculated, the intensities on the $hk0$ plane were extracted and plotted at their corresponding location in reciprocal space (Figure 4). The $hk0$ plots reveal some of the mosaicity in the heptapeptide crystals, as well as the presence of mosaic domains that appear to have different lattice constants (Figure 4A). The width of the Bragg reflections seems to be uncorrelated with the intensity or with the spatial frequency (distance to the center). The reflections are elongated in the azimuthal direction (Figure 4B), indicating a mosaic spread of $\sim 1.5°$ in the equatorial plane. Measurements of the widths of the Bragg reflections in the radial direction indicate a lateral coherence distance of the order of $\sim 150-300$ Å, consistent with the width of the crystallite domains measured by electron microscopy. Since the sampling in most of the electron diffraction tilt series was relatively coarse (1° to 3° steps between successive frames), measurement of reliable integrated intensities could not be made. Nevertheless, the peak intensity of observed reflections provided a crude estimate of their strength.

The electron diffraction spots are slightly thinner in the meridional direction ($\sim 1/200$ Å) than in the equatorial ($\sim 1/160$ Å), indicating that the correlation length is larger in the c-direction than in the $a-b$ plane. In the azimuthal direction we observe a half width corresponding to $\sim 1/140$ Å. The measurement in the azimuthal direction is independent of artifacts of the CCD detector used for the electrons. We found the width of the spots at half maximum to be variable and not clearly correlated with the intensity of the spot, or its corresponding spatial frequency. The domain size measurements by electron diffraction are in rough agreement with the values extracted from X-ray powder patterns, which show reflection widths corresponding to ~ 300 Å. These discrepancies can be attributed in part to the convergence of the beam used in the experiments, as well as to the presence of inelastic scattering.[14]

The order-to-order resolution of the camera used for X-ray powder diffraction at the SPring8 synchrotron facility was measured using a test sample made of ground calcium sulfate crystals. The full width at half maximum of the test sample was ~ 1200 Å, indicating that the width of the experimental lines was due to finiteness of the sample, and was not an instrumental artifact. The width of the reflections of the orthorhombic crystals was seen to increase very slightly with increasing resolution.

Model building

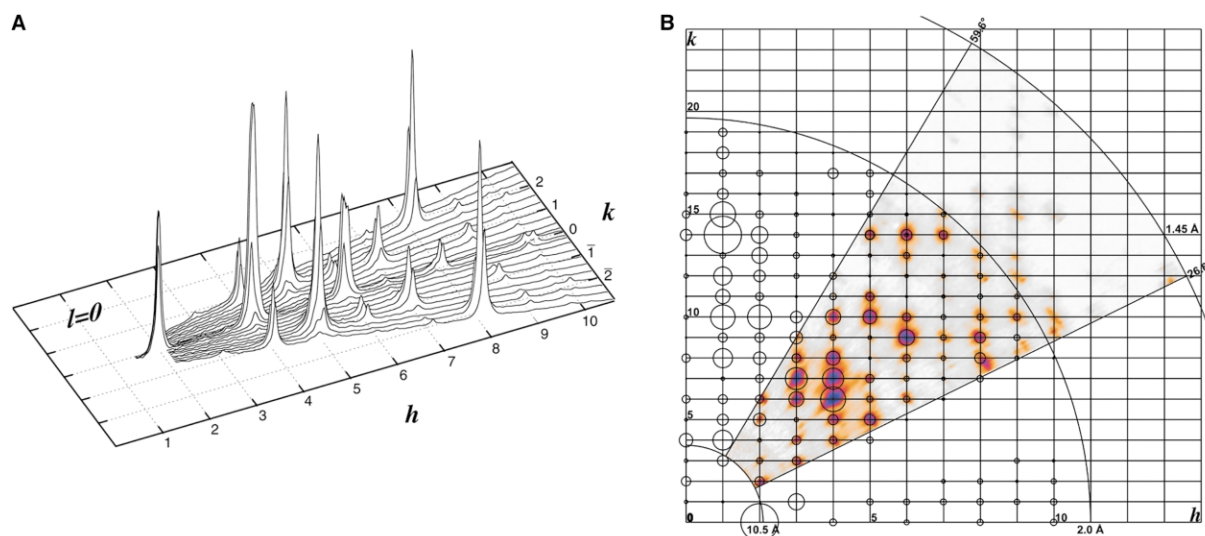There are a handful of reflections considerably stronger than most (Figure 4B). These reflections

Figure 4. Shapes of the Bragg reflections in reciprocal space. A, Surface plot of some of the *hk*0 reflections from a tilt series that included the *a** axis. Some reflections such as the 800 and 10 0 0 show split reflections, suggestive of a second lattice present in the diffraction pattern. B, Reconstruction of the *hk*0 reflections from a tilt series that spanned more than 45° (33 in the *hk*0 plane). The Bragg spots are generally extended in the angular direction. The streaks in the radial direction, noticeably mostly for the strong reflections, are due in part to the transfer function of the CCD detector.

point towards a model in which the peptide backbone is aligned nearly parallel with the *a*-axis, making an angle about 7° with *a*. However, when the models are compared to the diffracted intensities, the resemblance between model and data is rather poor, showing *R*-factors of the order of 30%. Other models with straight beta strands are possible (Figure 5), but models with curved beta strands have not been systematically explored. However, the evidently tight packing of the crystals implies pairing of aligned beta strand segments.

Discussion

Water content of the aggregates

The preservation of the crystalline order under solvent changes is a direct consequence of the highly anhydrous packing of the peptide. Density measurements[9] show that the peptide occupies 93% of the volume in the unit cell, which translates to about two to four water molecules per peptide. However, calculations of the molecular volumes using the typically observed volumes for Gly, Asn, Gln and Tyr in protein crystals,[15] suggest a peptide volume between 915 Å^3 and 936 Å^3, and consequently, between four and six water molecules per peptide in the unit cell. This discrepancy suggests that the side-chains in the peptide are forming hydrogen bonds directly with the side-chains from the neighboring peptide, largely excluding water in the process. A relatively large activation energy would be required to disrupt this network of hydrogen bonds, pointing to a possible explanation of the stability of the cross-beta structures.

Packing models

The class of models that we currently favor to describe the packing of the peptide molecules in the crystal has the peptide backbone nearly along the *a* axis, with a slight tilt of ~7° with respect to the *a* axis, in order to weaken the intensities along the *b* axis, while producing a strong (1,14,0) reflection. The side-chains in this class of model are nearly parallel with the *a*−*b* plane. The strong peak observed at 9.85 Å in the X-ray powder patterns of the wet samples, is due to the overlap of the 220 and the 040 reflections. However, in the patterns of the dry samples, the 040 and the 220 reflections are separated, and we can see that the 040 reflection contributes most of the intensity. This suggests that the β-sheets are connected along the *b* axis through side-chain contacts, spanning a distance ~9.85 Å per monomer in the *b* direction. There is little ambiguity about the nature of the peptide backbone structure viewed perpendicular to the *c* axis, since it is the regularly hydrogen bonded Pauling–Corey parallel β-sheet. The strongest reflection in both the electron diffraction and in the X-ray powder patterns occurs at 4.72 Å. From the electron diffraction data, we index this reflection as 021. In our model, this reflection arises from the stagger by half a unit cell that the 2-fold screw axis parallel with *b* conveys to the peptide molecule, but in other models it can be made to arise from a tilt of the beta strand out of the equatorial plane. The arrangement of the peptide monomers in the unit cell is suggestive of a pair of protofilaments, in which a protofilament consist of one of the pairs of β-sheets, which would form a spiral with a pitch of 4.86 Å, a width of ~30 Å and a thickness ~20 Å,
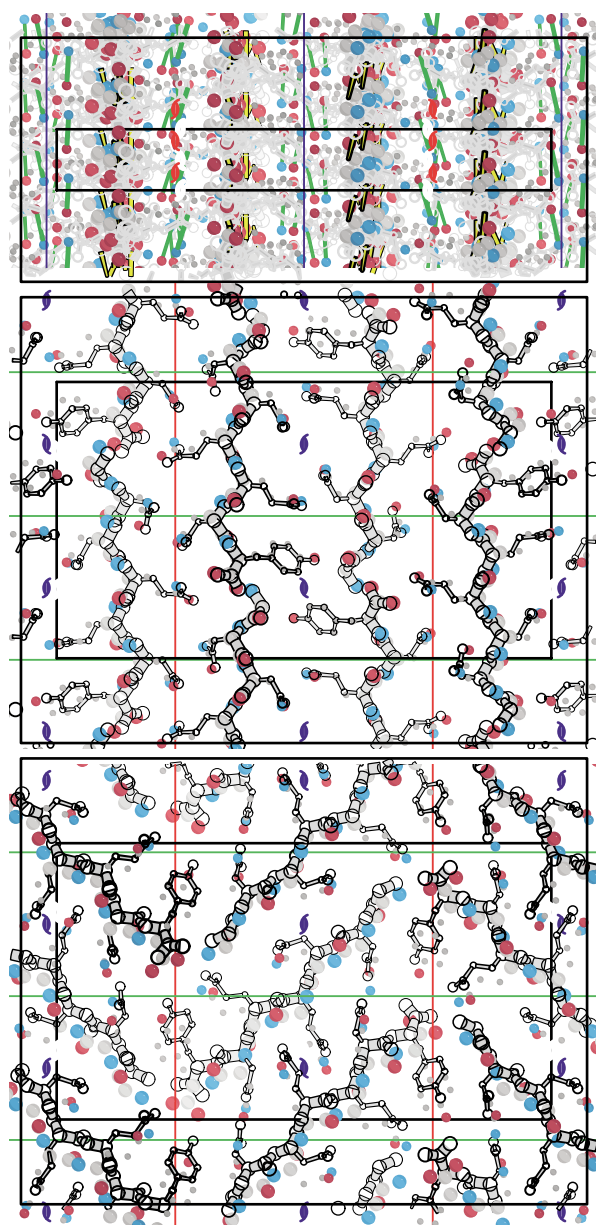
Figure 5. Two possible packing models for the peptide in the unit cell of the orthorhombic crystals. The top part of the Figure corresponds to the view along the backbone of the peptides showing the hydrogen-bonding network in cyan. The central frame of the Figure shows a model with the backbone of the peptide nearly along the *a* axis. This model is suggested to account for the strength of some reflections such as the 021, 1 14 0, and the 400, which are the strongest measured from the electron diffraction data. The bottom frame of the Figure shows a model with the peptide backbone aligned nearly diagonal to the *hk*0 plane and which is sterically plausible.

resembling the packing of β-sheets in pectate lyase.[16]

Comparisons of the peptide models against the electron diffraction intensities, have shown rather poor correlation. At first sight, it would seem that the presence of $P2_12_12_1$ symmetry, together with the small unit cell observed in the peptide crystals

should reduce the number of possible packing schemes of the peptide to a handful of configurations that satisfy the stereochemical constraints. However, it is possible to make a wide variety of models in which the strands are oriented with different angles in the $a-b$ plane, and still satisfy the symmetry of the crystals (Figure 5B). At present all the models that we have tried show an equally poor resemblance to the data, but when the side-chains are accommodated so as to minimize the energy of the crystal, a common feature observed is the presence of amide ladders, similar to those of the peptides associated with Huntington's disease[17] (Figure 5C).

One of the most interesting properties of this peptide, is the fact that it has eluded all efforts to produce large crystals suitable for single-crystal X-ray crystallography. A tendency to form crystals of limited size might be an inherent property of the β-sheet packing, since β-sheets have a natural tendency to curve, and therefore being in an extended conformation might introduce a cumulative strain that hampers the growth of large crystals, as observed for the crystals of sickle cell hemoglobin.[18]

The ultra fine and ultra intense X-ray beams from third generation synchrotron sources has been shown to allow the measurement of structure factors suitable to determine the atomic structure of protein crystals, using molecular replacement techniques combined with Rietveld and stereo-chemical restraint refinement.[19,20] However, such approach is unlikely to lead to success with our samples due to several circumstances. On the one hand, the limited size of the crystalline domains causes rather severe overlap on reflections corresponding to similar spatial frequencies. Furthermore, the ratio of b/a is almost exactly $\sqrt{3}$, and therefore, all the $(0, 2k, l)$ reflections are overlapped with the (h, h, l) reflections, with no trivial algorithm to discern their relative contributions. The overlap of reflections becomes a more severe problem at higher resolutions, and the increase in the width of the reflections as a function of resolution, even if marginal, only increases the challenges. In order to circumvent the problem of overlapped reflections belonging to lattice planes with different l values, we have attempted to induce preferential orientation of the crystals in the samples, but in that case the problem is to make sure that the diffracted intensity is measured properly. Determination of phase information has been hampered by the apparent impossibility to diffuse heavy atoms into the crystal lattice.

Electron diffraction data

The use of electron scattering data for *ab initio* structure analysis has several potential pitfalls, such as dynamical scattering, secondary scattering and crystal bending.[21] Dynamical diffraction simulations carried out using the program ncemss[22] on some of our tentative models, have suggested the

likelihood of a strong coupling between several Bragg reflections when they are simultaneously excited; that is, when they appear simultaneously on a given frame. This coupling makes the intensity measurement of the reflections to oscillate as a function of the thickness of the crystal, and since the crystal thickness is a parameter that we can only estimate, the measurement of coupled intensities is unreliable. Weaker reflections can be expected to have a nearly kinematic behavior.

All the information that we need to see the packing of the peptide in the crystal is contained in the $hk0$ reflections, since in the c direction the structure connected in a predictable manner by hydrogen bonds. We have collected electron diffraction intensities that sample the $hk0$ plane to ~ 2 Å, but some of the reflections show non-trivial departures from Friedel's symmetry, indicating a perturbation on the data, and therefore more experiments are needed to insure that the observed intensities are self-consistent. Once this is achieved and a more reliable model is produced, the electron diffraction data can be simulated incorporating multislice calculations of dynamical scattering as well as absorption effects to further refine the models.

This small peptide offers a unique system to study the molecular interactions that define the cross-beta structure in a detailed manner. The structure adopted by the peptide molecules in the crystals might turn out to be an unremarkable one; however, the importance of this system lies in the opportunity it provides to acquire direct structural information about the intramolecular contacts made by the monomers forming the aggregates, which might in turn provide an explanation to questions about their stability, and a much better understanding of their genesis.

Materials and Methods

Peptide synthesis and crystallization

The peptide (Gly-Asn-Asn-Gln-Gln-Asn-Tyr) has been synthesized at the Chemistry Department of Florida State University and at the Biopolymer Synthesis Center of the California Institute of Technology using F-moc and T-boc chemistry, respectively. The peptide was cleaved from the resin with trifluoroacetic acid, precipitated adding ethyl ether, recovered by centrifugation and lyophilized. Some of the peptide was later purified by reverse phase chromatography, dissolving the peptide in 8 M guanidine hydrochloride, and eluting with a 0–70% (v/v) acetonitrile gradient. The fractions containing the peptide were immediately dipped in liquid nitrogen and lyophilized. The purity of the powder was assessed by mass spectrometry to be greater than 98%, and sequencing of the peptide showed it to have the correct amino acid composition. Samples of the lyophilized peptide were examined by X-ray diffraction to assess their amorphous structure before adding water. Aqueous suspensions containing microcrystals were prepared as described by Balbirnie *et al.*[9] Solubilization of the peptide in hexafluoro-2-propanol (HFIP) and precipitation by

ether produces a powder that yields an alternative crystal form when hydrated.

Electron microscopy

Ice-embedded samples of fibers and microcrystals for electron microscopy were prepared in the standard way[23] using perforated carbon grids. A 4 μl drop of sample (~ 2 mg/ml) was placed on a glow-discharged grid, and dipped in liquid ethane after blotting the excess solution. The samples were then transferred to the microscope on a Gatan model 626 cryoholder (Gatan Inc., Pleasanton, CA) and observed on a Philips CM30FEG microscope operating with an accelerating voltage of 300 kV. Images were collected using defocus values from ~ -500 nm to -3 μm.

Electron diffraction of microcrystals

A 4 μl drop of sample (1:4 crystal suspension) was placed on a copper grid with a continuous carbon film for about two minutes. The excess solution was then blotted and a drop (4 μl) of 1% (w/v) dextrose was applied to the grid and blotted immediately. The grid was then left to dry for about ten minutes before inserting into the microscope. In order to have an internal calibration standard, we used evaporated gold on some samples.

The electron diffraction patterns were collected using a slightly convergent beam to restrict the irradiated area to ~ 2 μm in diameter. A 50 μm selected area aperture was used to allow only electrons being diffracted from a target area ~ 500 nm in diameter. Once a crystal was found, a diffraction pattern was collected, and if this pattern appeared to arise from a single crystal with no evident polycrystallinity, a tilt series was collected, with the number of patterns recorded being constrained by radiation damage. A diffraction pattern was collected at zero degrees at the end of the process, to assess the radiation damage. Some of the tilt series were collected using small angular increments in order to determine the shape of the Bragg reflections in reciprocal space.

The electron diffraction data were initially collected on Kodak SO163 film plates with a Philips CM30FEG microscope using an accelerating voltage of 300 kV, and later on a JEOL 400 microscope fitted with a 2048 × 2048 pixel slow-scan CCD camera (Gatan, Inc.) at the Lawrence–Berkeley laboratory, with an accelerating voltage of 400 kV, and nominal camera length values between 1000 mm and 2500 mm.

Mapping the electron diffraction data to reciprocal space

The unit cell dimensions determined from the X-ray powder patterns were used to find the hkl values of two linearly independent low-resolution reflections, together with their corresponding Friedel pairs. The variation in the intensity of the Friedel pairs was taken as an indicator of distance to the Ewald sphere, which allowed a first estimation of the rotation matrix and camera length for each diffraction pattern. These parameters were refined as more reflections were included. In some of the tilt series, the presence of either a^* or b^* in a pattern was evident, providing direct measurements of the ratios $|a*|/|c*|$ or $|b*|/|c*|$ for that series. Since c^* shows little variation experimentally, we were able to find accurate values for a^* and b^*, even if no calibration standard had

been included with the sample. Once the rotation matrix for a given diffraction pattern was determined, the data were mapped from detector to reciprocal space by assigning each pixel in the diffraction pattern to a voxel in reciprocal space corresponding to the location of the Ewald sphere. In order to subtract the strong background due to the inelastically scattered electrons, each electron diffraction pattern was centered and rotated to have the *hk*0 reflections in the horizontal direction. A strip of data containing the center was excised at 15° and taken as the background to be subtracted from its corresponding pattern.

X-ray powder diffraction

Samples for X-ray powder diffraction were prepared under different solvent conditions by placing a small drop of crystal suspension on a quartz capillary, and centrifuging the capillary softly to sediment the crystals to the bottom. After collecting an X-ray pattern at room temperature, a cold nitrogen stream was used to lower the temperature of the sample to ~ 100 K, and another diffraction pattern collected. The sample was then brought to room temperature and the excess water removed. Pure ethanol was added to the capillary, the suspension stirred, centrifuged and the supernatant (ethanol) removed. The process was repeated once, and the sample placed in the X-ray beam to collect powder diffraction data at room and liquid nitrogen temperatures. The same procedure was performed replacing ethanol with acetone. In order to test the effects of drying on the microcrystals, a sample of crystalline suspension was placed in an evacuated desiccator containing P_2O_5 for three days. X-ray diffraction patterns were then collected at room and liquid nitrogen temperatures. Water was added to the dried powder samples and once more, diffraction patterns collected at ~ 300 and 100 K. The X-ray powder data were collected with a Rigaku generator, using a copper anode and recorded with either an R-axisII image plate detector or a MAR research CCD detector.

High-quality powder diffraction data were collected from wet and dried orthorhombic crystals at the SPring8 synchrotron facility in Hyogo, Japan, using an evacuated camera with a specimen to detector distance of 1000 mm, housing a 200 mm × 400 mm image plate (Fuji Corp., Kyoto, Japan). In order to minimize the X-ray scattering due to air near the specimen, a 0.5 mm square guard aperture was placed next to the specimen. Images of the direct beam (attenuated with a nickel foil) were collected in order to determine the beam profile. Additionally, patterns of $CaSO_4$ were collected to calibrate the camera length and to determine the order-to-order resolution of the experimental setup. In order to record higher resolution data, more patterns were collected using an *R*-axis IV image plate detector with a specimen-to-detector distance of 420 mm. The wavelength used for all the synchrotron experiments was 1 Å.

Processing of the X-ray powder diffraction patterns

The powder diffraction patterns were centered, averaged circularly and corrected for the effects of the sphere of reflection in order to determine the radial diffracted intensity profile. The reflections corresponding to spatial frequencies lower than ~ 5 Å, which belong to the *hk*0 plane, were indexed on a two-dimensional lattice and

then the appropriate *c*-dimension was used to account for higher resolution non-equatorial reflections.

References

1. Astbury, W. T., Dickinson, S. & Bailey, K. (1935). The X-ray interpretation of denaturation of the seed globulins. *Biochem. J.* **29**, 2351–2360.
2. Rudall, K. M. (1952). The proteins of the mammalian epidermis. *Advan. Protein Chem.* **7**, 253–290.
3. Fraser, R. D. B. & MacRae, T. T. (1973). *Conformations in Fibrous Proteins and Related Synthetic Polypeptides*, Academic Press, New York.
4. Kirschner, D. A., Inouye, H., Duffy, L. K., Sinclair, A., Lind, M. & Selkoe, D. J. (1987). Synthetic peptide homologous to beta-protein from alzheimer-disease forms amyloid-like fibrils *in vitro*. *Proc. Natl Acad. Sci. USA*, **84**, 6953–6957.
5. Benzinger, T. L. S., Gregory, D. M., Burkoth, T. S., Miller-Auer, H., Lynn, D. G., Botto, R. E. & Meredith, S. C. (1998). Propagating structure of Alzheimer's beta-amyloid (10–35) is parallel beta-sheet with residues in exact register. *Proc. Natl Acad. Sci. USA*, **95**, 13407–13412.
6. Halverson, K., Fraser, P. E., Kirschner, D. A. & Lansbury, P. T. (1990). Molecular determinants of amyloid deposition in alzheimer's disease. Conformational studies of synthetic beta-protein fragments. *Biochemistry*, **29**, 2639–2644.
7. Serpell, L. C. & Smith, J. M. (2000). Direct visualisation of the β-sheet structure of synthetic Alzheimer's amyloid. *J. Mol. Biol.* **299**, 225–231.
8. Geddes, A. J., Parker, K. D., Atkins, E. D. T. & Brighton, E. (1968). 'Cross-β' conformation in proteins. *J. Mol. Biol.* **32**, 343–358.
9. Balbirnie, M., Grothe, R. & Eisenberg, D. S. (2001). An amyloid-forming peptide from the yeast prion Sup35 reveals a dehydrated b-sheet structure for amyloid. *Proc. Natl Acad. Sci. USA*, **98**, 2375–2380.
10. Cowley, J. (1984). *Diffraction Physics*, North Holland, Amsterdam.
11. Otwinowski, Z. & Minor, W. (1996). Processing of X-ray diffraction data collected in oscillation mode. *Methods Enzymol.* **276**, 307–326.
12. Leslie, A. G. W. (1999). Integration of macromolecular diffraction data. *Acta Crystallog. sect. D*, **55**, 1696–1702.
13. Dimmeler, E. & Scroeder, R. R. (2000). Global least-squares determination of Eulerian angles from single electron diffraction patterns of tilted crystals. *J. Appl. Crystallog.* **33**, 1088–1101.
14. Spence, J. C. H. (1993). On the accurate measurement

of structure-factor amplitudes and phases from electron diffraction. *Acta Crystallog. sect. A*, **49**, 231–260.

15. Tsai, J., Taylor, R., Chothia, C. & Gerstein, M. (1999). The packing density in proteins: standard radii and volumes. *J. Mol. Biol.* **290**, 253–266.

16. Yoder, M. D., Keen, N. T. & Jurnak, F. (1993). New domain motif—the structure of pectate lyase-C, a secreted plant virulence factor. *Science*, **260**, 1503–1507.

17. Perutz, M. (1999). Glutamine repeats and neurodegenerative diseases: molecular aspects. *Trends Biochem. Sci.* **24**, 58–63.

18. Mu, X.-Q., Makowski, L. & Magdoff-Fairchild, B. (1998). Analysis of the stability of hemoglobin S double strands. *Biophys. J.* **74**, 655–668.

19. Von Dreele, R. B., Stephens, P. W., Smith, G. D. & Blessing, R. H. (2000). The first protein crystal structure determined from high-resolution X-ray powder diffraction data: a variant T3R3 human insulin–zinc complex produced by grinding. *Acta Crystallog. sect. D*, **56**, 1549–1553.

20. Von Dreele, R. B. (2001). Binding of *N*-acetylglucosamine to chicken egg lysozyme: a powder diffraction study. *Acta Crystallog. sect. D*, **57**, 1836–1842.

21. Dorset, D. (1995). *Structural Electron Crystallography*, Plenum Press, New York.

22. Kilaas, R. & Gronsky, R. (1983). Real space image simulation in high resolution electron microscopy. *Ultramicroscopy*, **11**, 289–298.

23. Adrian, M., Dubochet, J., Lepault, J. & McDowall, A. W. (1984). Cryo-electron microscopy of viruses. *Nature*, **308**, 32–36.

Edited by F. E. Cohen